Design and Analysis of an Axial Flux Magnetically Geared Generator

Matthew Johnson
IEEE Student Member
mjohnson11@tamu.edu

Matthew C. Gardner
IEEE Student Member
gardner1100@tamu.edu

Hamid A. Toliyat
IEEE Fellow
toliyat@tamu.edu

Advanced Electric Machines & Power Electronics Lab
Texas A&M University
College Station, TX

***Abstract*—Axial flux magnetically geared machines offer the potential to achieve exceptional torque densities at high diameters. This work proposes a topology for an axial flux magnetically geared machine, in which the electric machine is placed in the bore of the axial flux magnetic gear. This new topology offers the advantage of correctly matching the size of the electric machine to its required torque without increasing the volume of the system beyond that of the magnetic gear. A proof of concept prototype with a torque density of 7.8 kN·m/m^3 was designed, fabricated, and tested to evaluate the novel topology. A less conservative alternate design capable of achieving 60.6 kN·m/m^3 was also simulated to demonstrate the topology's potential for high torque densities, and even higher torque densities can be reached at larger scale designs.**

Keywords—Axial flux, direct drive, finite element analysis, magnetic gear, magnetically geared machine, torque density

I. Introduction

Over the past two decades, magnetic gears have attracted attention as a possible replacement for their mechanical counterparts [1]-[4]. Instead of achieving the gearing action through the physical contact between teeth, magnetic gears create the same behavior through the modulated interaction between the flux generated by magnets on the input and output rotors. This contactless operation provides a plethora of potential advantages, such as reduced maintenance, inherent overload protection, improved reliability, decreased noise, and physical isolation between shafts. As a result of these promising characteristics, magnetic gears have drawn interest for use in several industrial applications including wind turbines [5], wave energy generation [6], traction drives in electric vehicles [7], and underwater propulsion [8].

While most existing works focus on variations of the coaxial radial flux magnetic gear [1]-[4], the axial dual of this topology has been proposed [9] and received some recent interest [10]-[12], including one study which developed an experimental prototype [13]. Both the radial and axial flux topologies operate on the same fundamental principles [1], [9] which are characterized by (1) - (2). Either topology consists of a high speed rotor (HSR) with a relatively small number of permanent magnet (PM) pole pairs (P_{HS}) and a low speed rotor (LSR) with a larger number of permanent magnet pole pairs (P_{LS}). The two permanent magnetic rotors are separated by an intermediate fixture with the appropriate number of ferromagnetic modulators (Q_M) which modulate the fields from the permanent magnets and allow for smooth transmission of torque at a fixed gear ratio. For the gear to function properly, the number of modulator segments must be related to the number of magnetic pole pairs on the two rotors according to (1). In the simplest mode of operation, the modulators are fixed while the high and low speed permanent magnet rotors rotate freely at ω_{HS} and ω_{LS} respectively, resulting in the gear ratio given by (2). Alternatively, the modulators can be rotated instead of the high magnet pole count assembly, which increases the magnitude of the gear ratio given in (2) by one and changes the sign of the gear ratio.

$$Q_M = P_{LS} + P_{HS} \tag{1}$$

$$\text{Gear Ratio} = \frac{\omega_{HS}}{\omega_{LS}} = \frac{-P_{LS}}{P_{HS}} \tag{2}$$

As a natural extension of a passive magnetic gear, a magnetically geared machine (MGM) directly integrates a magnetic gear with a conventional low torque, high speed electric machine, producing a single compact device which combines the benefits of a magnetic gear and the simplicity of a traditional direct drive machine. The literature on magnetically geared machines is even more heavily tilted towards radial field systems [14]-[17]. Although there are several different proposed radial flux magnetically geared machine (RFMGM) topologies, the two most promising appear to be an outer stator configuration and the inner stator arrangement illustrated in Fig. 1. The outer stator RFMGM has the simpler mechanical structure out of these two topologies, having two air gaps rather than three air gaps, but the stator is inherently oversized, which constrains the torque densities that can be achieved. Despite this limitation, the outer stator RFMGM dramatically outperforms traditional direct drive machines and is capable of achieving torque densities in excess of 60 kN·m/m^3 [14]. The inner stator RFMGM is a slightly more complex topology from a mechanical standpoint, but it yields a more natural pairing of the stator and gear sizes resulting in even higher torque densities on the order of 100 – 130 kN·m/m^3 [16], [17].

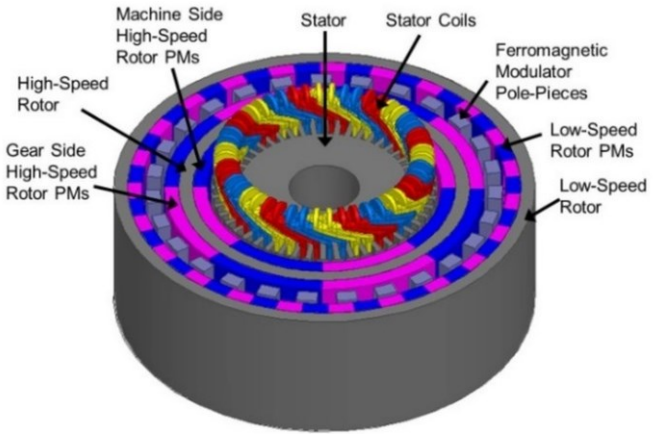

Fig. 1. Inner Stator Radial Flux Magnetically Geared Machine

One significant appeal of axial flux magnetic gears can be observed through a simplistic theoretical analysis. For a radial topology with constant average air gap shear stress, torque increases with the square of the radius. This occurs because the air gap area increases linearly with radius, increasing the tangential forces linearly, and the torque arm of those tangential forces increases linearly with radius. However, for an axial topology with constant average air gap shear stress, the torque increases with the cube of the radius. This occurs because the air gap area increases with the square of the radius and the average torque arm increases linearly with the radius. Since volume increases with the square of the radius, the axial field gear can theoretically achieve a torque density that increases linearly with the radius, while the radial field gear's torque density is ideally independent of the radius. This scaling principle causes axial field magnetic gears to favor designs with large outer diameters and short stack lengths. While these trends are subject to practical limiting concerns, such as the large axial forces of the axial field gear and the associated mechanical design requirements, the lack of experimental axial field magnetic gear and magnetically geared machine prototypes means that the implications of these issues are not well understood.

Only four known studies of axial flux magnetically geared machines (AFMGMs) have been published [18]-[22]. The first type suffers from an inherently low torque density because it replaces the high speed rotor magnets with stationary coils [18], [19]. The second topology, shown in Fig. 2, appears to have much better potential despite the disappointing performance of the first prototype, which was caused by various mechanical and leakage flux issues [22]. However, while this topology does remove the need for a shaft connecting the electric machine to the magnetic gear, it is much closer to a series connection of the two devices than it is to the compact integration accomplished by the RFMGM topology shown in Fig. 1. Furthermore, because the axial field magnetic gear must transmit a much larger amount of torque than the axial machine, it requires a larger outer radius, which agrees with the results found in [21] and [22]. This consideration suggests that the axial field machine and axial field magnetic gear will tend to be mismatched in size.

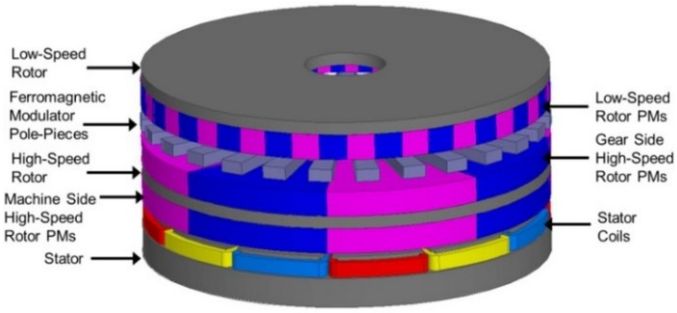

Fig. 2. Series Connected Axial Flux Magnetically Geared Machine

On top of the size matching issues, the series connected AFMGM topology in Fig. 2 has the undesirable characteristic that the addition of the axial field machine increases the overall size of the device, unlike the RFMGM topology in Fig. 1. The significance of this is evidenced by the fact that [21] reports a volumetric torque density of 105 kN·m/m^3 for the topology, based only on the gear volume; unfortunately, if the generator volume (not including end windings) is also considered, then the torque density decreases by about 50% [22].

II. Proposed Topology

This work continues to fill the void of experimental results for axial field magnetically geared systems by proposing, constructing, and analyzing the new compact AFMGM topology illustrated in Fig. 3 and Fig. 4. This design consists of an axial flux permanent magnet machine located concentrically in the radial bore of an axial flux magnetic gear. The high speed rotors of both the electrical machine and the gear are connected together to form a single mechanical structure, as depicted in Fig. 4. The relationship between the high speed rotor magnet pole pair count (P_{HS}), low speed rotor magnet pole pair count (P_{LS}), and modulator pole pieces count (Q_M), as well as the resulting gearing ratio, are still described by (1) and (2), respectively. The axial flux permanent magnet generator pole count can be selected independently of the gear pole counts, provided that there is a large enough radial gap between the two subsystems to ensure isolation.

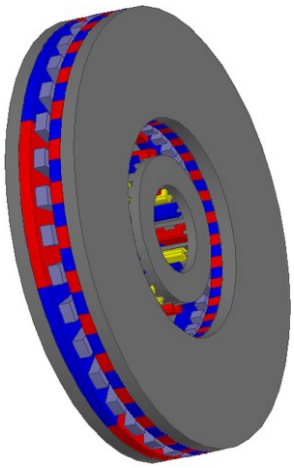

Fig. 3. Proposed Compact Axial Flux Magnetically Geared Machine Topology

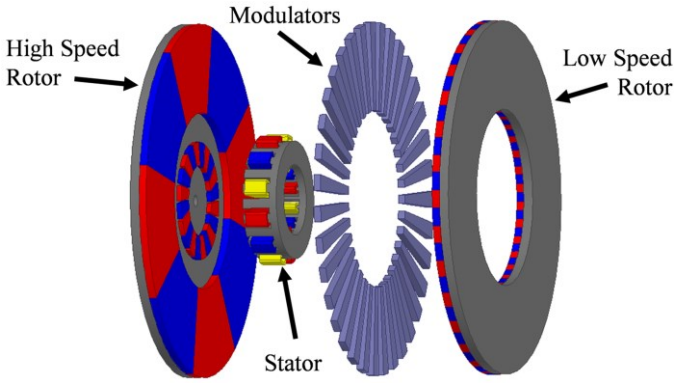

Fig. 4. Exploded View of the Proposed Compact AFMGM

When the compact AFMGM is operated as a generator, the external motion source turns the gear's LSR. The LSR magnets then interact with the HSR magnets through the modulators to produce motion in the HSR according to the gear ratio given by (2). Because the gear's HSR and the generator's rotor are a single mechanical structure, the torque exerted on the gear HSR magnets also rotates the generator magnets. The motion of the generator magnets then electrically excites the stator windings. As with conventional machines, the system can also be driven in the inverse configuration as a motor.

Placing the axial field generator inside the bore of the gear prevents the increase in volume caused by the series connection of the generator to the gear in the original topology. This makes use of the empty space inside of the axial gear which is unused or poorly used in the original topology. As a result of this change, the total volume consumed by the compact AFMGM is identical to that required for the corresponding passive axial field gear (although additional limitations are now placed on the inner radius of the gear). The compact topology also allows the generator to inherently use a smaller outer radius than the magnetic gear, which is consistent with their natural design points since the generator is a low torque, high speed machine and the gear is high torque, low speed device. Another small, but potentially significant advantage of this topology is that the HSR back iron can be thinner than in the original magnetically decoupled version of the series connected design, because it no longer has to isolate or accommodate flux from magnets on both sides. All of these benefits are independent of whether the high magnet pole count disk or the modulators are allowed to rotate.

III. Design of Prototype

In order to experimentally evaluate the proposed topology, a small scale prototype was designed and fabricated. Due to time and cost constraints, the rotor and tape wound laminated stator from a commercially available axial field PM machine were used as the integrated generator in the compact AFMGM. This repurposed machine, which is shown in Fig. 5, is rated for 3.4 N·m at a speed of 2800 rpm (a power of 1 kW). While this machine is suboptimal for use in the magnetically geared machine topology, hindering the performance of the AFMGM, it does not prevent the prototype from being useful for addressing magnetic and mechanical design considerations and for experimental evaluation of the proposed topology and magnetically geared machines in general.

Due to time and cost considerations, the magnetic gear portion of the prototype was intentionally designed for ease of fabrication and for low cost rather than for optimal performance. Future work could be performed to create an optimized version of the topology; however, the parametric study defined in Table I was conducted using 3D finite element analysis in ANSYS Maxwell to develop a conservative gear prototype and illustrate key design trends. In this sweep, the derived parameter, G_r, is the approximate (nearest integer) desired gear ratio and is used to relate the number of low speed rotor pole pairs to the number of high speed rotor pole pairs with (3). This maintains a high least common multiple between P_{HS} and P_{LS}, which reduces the gear's torque ripple [5]. A second derived parameter, K_R, relates the inner radius of the gear to its outer radius according to (4). Furthermore, the LSR magnet thickness is limited to not exceed the HSR magnet thickness to ensure that most of the magnet material is placed on the rotor with fewer poles and less leakage flux. Similarly, the LSR back iron is limited to not exceed the HSR back iron in thickness. For all designs, demagnetization was analyzed in the static simulations by evaluating the percentage of the magnet bodies operating at flux densities below the knee point of their demagnetization curves at 20 °C. While this neither comprehensively quantifies the full extent of demagnetization during operation nor addresses demagnetization's temperature dependence, it does indicate which designs are most susceptible to demagnetization. To that end, the 153 designs with more than 1% of the magnet volume operating below the knee point were removed from the population of 6480 designs. For most reasonable designs, this is typically not a significant issue at normal operating temperatures due to the reluctance of the two air gaps and the high coercivity of NdFeB magnets.

$$P_{LS} = G_r \times P_{HS} + 1 \tag{3}$$

$$R_{in} = K_R \times R_{out} \tag{4}$$

TABLE I. Axial Field Magnetic Gear Parametric Design Sweep

Name	Description	Values	Units
G_r	Nearest integer gear ratio	6, 9, 12	
P_{HS}	HSR pole pairs	2, 3, 4, 5	
R_{out}	Outer radius	70, 90, … 150	mm
K_R	Ratio of inner and outer radii	0.5, 0.625, 0.75	
T_{HSBI}	HSR back iron thickness	5, 10, 20	mm
T_{HSPM}	HSR magnet thickness	3.18, 6.35, 12.7	mm
T_{AG}	Air gap thicknesses	3	mm
T_{Mods}	Modulator thickness	6	mm
T_{LSPM}	LSR magnet thickness For T_{HSPM} = 3.18 mm For T_{HSPM} = 6.35 mm For T_{HSPM} = 12.7 mm	 3.18 3.18, 6.35 3.18, 6.35, 12.7	mm
T_{LSBI}	LSR back iron thickness For T_{HSBI} = 5 mm For T_{HSBI} = 10 mm For T_{HSBI} = 20 mm	 5 5, 10 5, 10, 20	mm

(a) (b)

Fig. 5. (a) Tape Wound Stator and (b) Rotor of Axial Flux PM Machine

Fig. 6 shows the variation of the maximum volumetric torque density (within this parametric sweep) with the gear ratio for different HSR magnet thicknesses. This demonstrates that within the evaluated design space the maximum achievable volumetric torque density of the gear decreases as the gear ratio increases beyond approximately 6. While the use of a larger gear ratio increases the necessary volume of the gear, it decreases the integrated machine size by lowering its torque requirement. Thus, a true system level optimization must involve varying the design of both the integrated machine and the gear as the gear ratio changes. Fig. 6 also illustrates that increasing the magnet thicknesses increases the torque density, but with diminishing returns.

Another important design parameter is the back iron thickness, which impacts the containment of magnetic flux, the torque rating (and torque density), and the efficiency. Fig. 7 illustrates the effects of pole count and the ratio of back iron to magnet thicknesses on the leakage flux density axially beyond the back irons. Flux leakage on both the HSR and LSR sides is heavily influenced by the HSR pole count and HSR magnet thickness. This occurs because the HSR magnets' lower order spatial flux harmonics span longer paths than the higher order harmonics from the LSR magnets. Also, higher pole counts decrease the span of the flux paths, decreasing leakage flux for a given back iron thickness. Fig. 8 shows the effect of the HSR back iron thickness on torque density. While a thicker back iron increases the torque by accommodating more flux, it also increases the active volume. Thus, oversizing the back iron beyond the thickness necessary to accommodate most of the flux actually decreases the torque density.

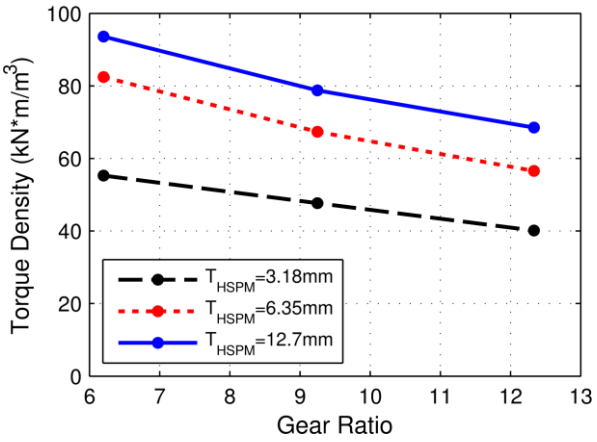

Fig. 6. Maximum Volumetric Torque Density vs. Gear Ratio for Different Magnet Thicknesses

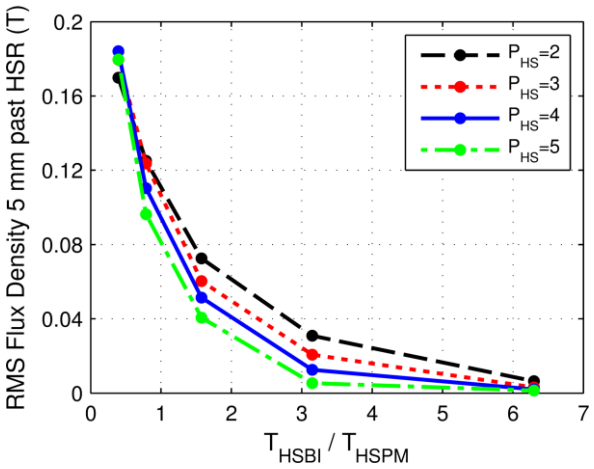

(a)

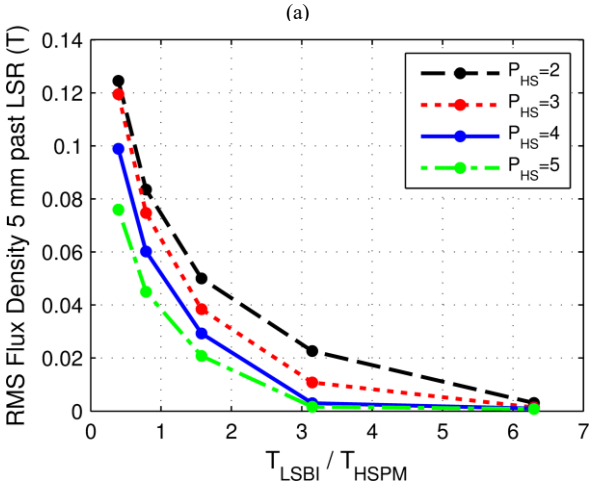

(b)

Fig. 7. Worst Case Leakage Flux Density Variation with HSR Pole Pairs, (a) HSR Back Iron to HSR Magnet Thicknesses Ratio, and (b) LSR Back Iron to HSR Magnet Thicknesses Ratio with an LSR Magnet Thickness of 3.18 mm

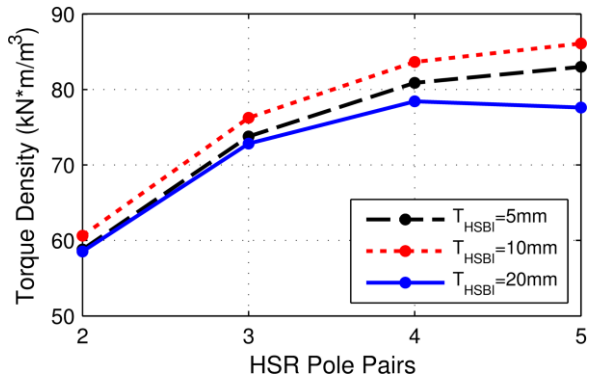

Fig. 8. Impact of HSR Pole Pair Count and Back Iron Thickness on Maximum Volumetric Torque Density

Fig. 9 shows the volumetric torque density for the set of points versus the corresponding low speed rotor stall torque. This illustrates that the maximum achievable torque density increases as the radius (and, thus, torque) increases, which is in accordance with axial field magnetic gear scaling principles presented in the introduction. It also implies that applications

requiring higher torque can expect to achieve even higher active volumetric torque densities. This is an important principle to consider when comparing different axial field magnetic gear designs presented in the literature.

Axial forces are a concern for axial field machines, especially magnetic gears. Fig. 10 shows the axial forces on the two rotors for different potential design points, and Fig. 11 shows the axial forces on the modulators. From Fig. 10, it is evident that the axial forces on the two rotors tend to increase with the required torque. However, because the axial force on the modulators is the difference between the axial forces on the two rotors (in accordance with Newton's 3rd law), designs with small total axial forces on the modulators can be achieved even for high torques, as illustrated in Fig. 11. This approach can be used to simplify the mechanical requirements of the support structure which holds the modulators in place.

The axial force data presented in Fig. 10 and Fig. 11 represents the forces corresponding to the maximum torque angle position. Fig. 12 and Fig. 13 illustrate the variation of the simulated torques and axial forces on the various bodies with the torque angle for the conservative prototype design. These graphs demonstrate that the maximum torque angle corresponds to intermediate axial force values. Thus, while Fig. 10 and Fig. 11 do not indicate the maximum axial forces on the bodies, they do indicate the general force trends.

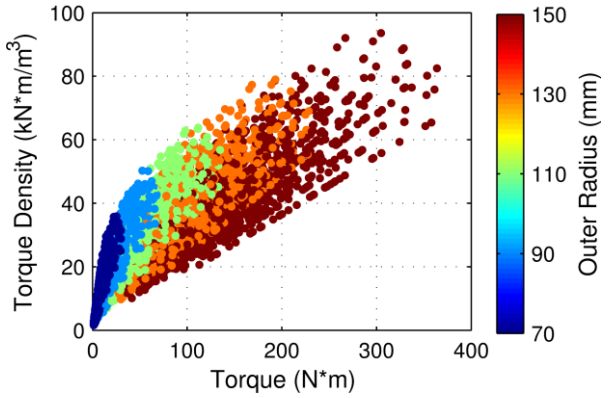

Fig. 9. Volumetric Torque Density vs. Torque Rating

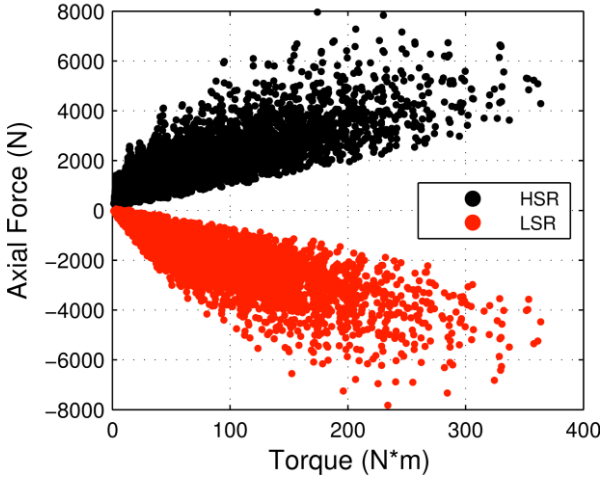

Fig. 10. Axial Forces on Rotors vs. Torque at Maximum Torque Angle

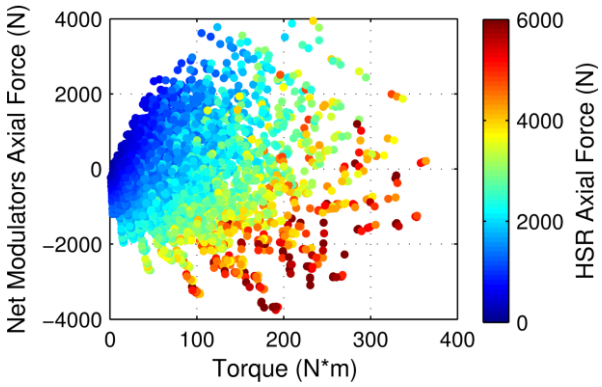

Fig. 11. Axial Force on Modulators vs. Torque at Maximum Torque Angle

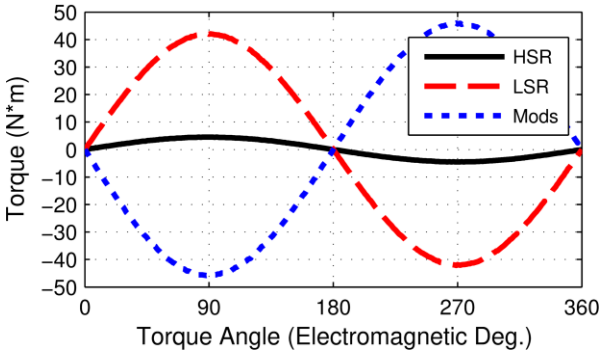

Fig. 12. AFMGM Prototype Simulated Torque Characteristics Curves

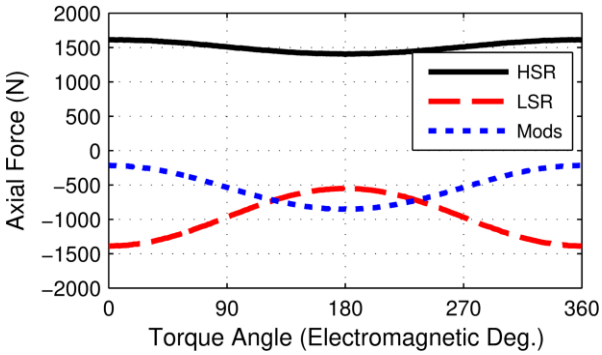

Fig. 13. AFMGM Prototype Simulated Axial Force Characteristics Curves

In addition to the experimental prototype, a more competitive theoretical magnetic gear design was simulated using a 3D FEA model to demonstrate the high torque densities that can be achieved by the topology. The differences between the prototype and the higher torque density design are simply intended to realistically reflect the superior manufacturing capabilities available in an industrial setting. This less conservative design is based on using the same commercially available stator and rotor for the integrated machine and still achieves the necessary magnetic isolation between the integrated machine and the magnetic gear. Table II shows the design parameters and ratings for both the fabricated prototype and the more aggressive design. Note that the dimensions of the integrated machine constrain the dimensions of the magnetic gear and that the torque rating of the integrated machine limits the volumetric torque density of the AFMGM.

Significant additional improvements could be achieved with the freedom to perform system level optimization of both the magnetic gear and the integrated machine.

IV. Mechanical Design

In order to quickly produce a working prototype for this novel topology, ease of fabrication and assembly was prioritized over performance. This approach is reflected in part by the large size of the air gaps, thickness of the modulators, common sizing of the back irons, and the large radial gap between the magnetic gear and the integrated machine, all of which are summarized in Table II. Additionally, the magnetic design was selected to reduce the axial load on the modulators structure. Throughout the mechanical design process, an ANSYS 3D mechanical FEA model was used with the forces from Maxwell 3D electromagnetic simulations to verify that static deformations were well within acceptable tolerances. A cutaway view of the resulting prototype is displayed in Fig. 14, and an exploded view is provided in Fig. 15. The completed prototype is shown in Fig. 16 on its testbed with the LSR connected to a DC motor, which is used as a prime mover.

TABLE II. DESIGN PARAMETERS AND RATINGS FOR AFMGM DESIGNS

Parameters and Ratings	Prototyped Design	Simulated Design
Gear Ratio	9.33	30.33
Stator Outer Diameter	100 mm	100 mm
End Winding Outer Diameter	120 mm	120 mm
Stator Stack Length	30 mm	30 mm
Integrated Machine Air Gap	2 mm	1 mm
Integrated Machine PM Thickness	4 mm	4 mm
Integrated Machine Back Iron Thickness	3 mm	3 mm
Stator Tooth Count	24	24
Integrated Machine Pole Pairs	10	10
Stator Current Density	6.3 A_{RMS}/mm^2	4.7 A_{RMS}/mm^2
Gear Inner Diameter	195 mm	160 mm
Gear Outer Diameter	260 mm	239 mm
HSR Pole Pairs	3	3
HSR Back Iron Thickness	20 mm	12 mm
HSR Magnet Thickness	6.35 mm	8 mm
Modulator Thickness	18 mm	6 mm
LSR Magnet Thickness	3.175 mm	4 mm
LSR Back Iron Thickness	20 mm	6 mm
Gear High Speed Side Air Gap	4.8 mm	1 mm
Gear Low Speed Side Air Gap	3.9 mm	1 mm
Gear Magnet Grade	NdFeB N42	NdFeB N42
LSR Pullout Torque	42.2 N·m	105.9 N·m
Rated LSR Speed	300 rpm	92 rpm
AFMGM Power	1 kW	1 kW
AFMGM Volumetric Torque Density	7.8 $kN·m/m^3$	60.6 $kN·m/m^3$
Gear Volumetric Torque Density	10.4 $kN·m/m^3$	62.2 $kN·m/m^3$

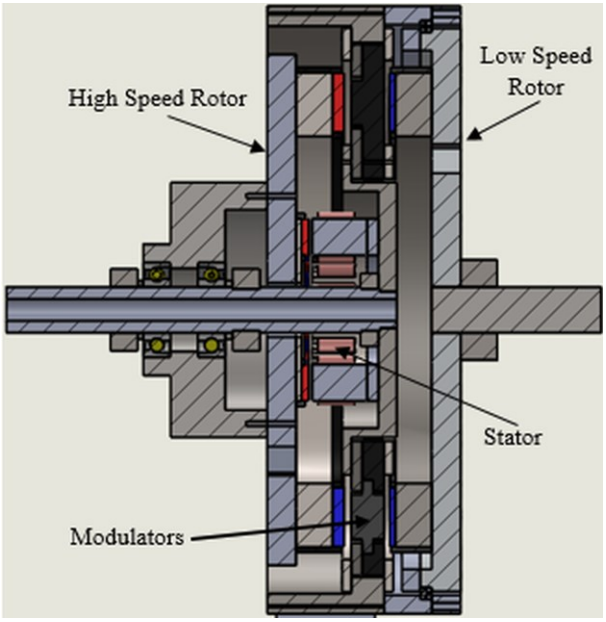

Fig. 14. Cutaway View of AFMGM Prototype

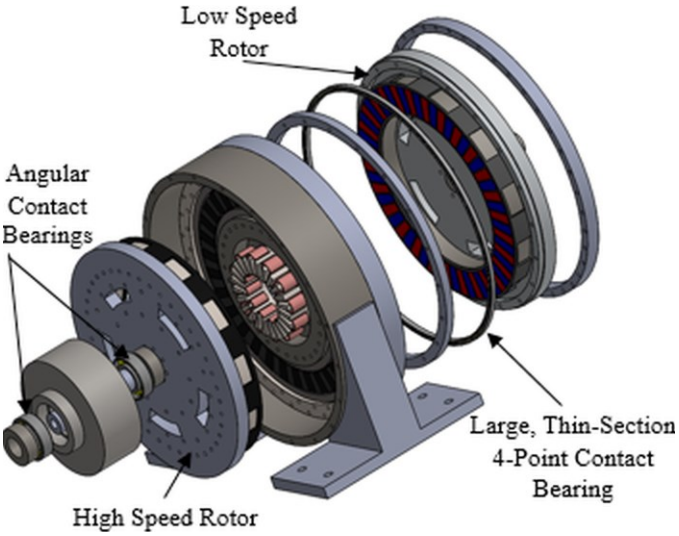

Fig. 15. Exploded View of AFMGM Prototype

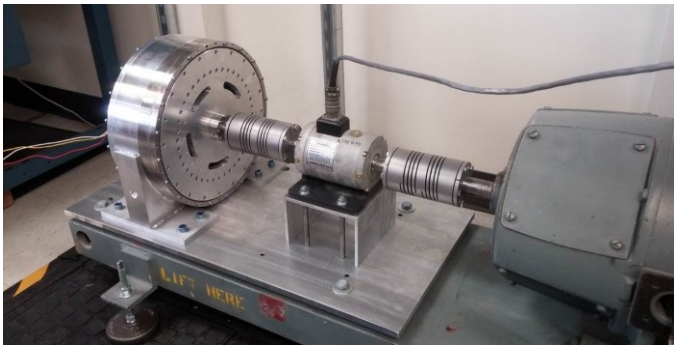

Fig. 16. AFMGM Prototype on Testbed

As indicated in Fig. 15, two angular contact ball bearings were used to support the high speed rotor. The bearings were

oriented in opposite directions to handle axial forces in either direction. While the HSR is always attracted towards the LSR in normal operation, forces in the opposite direction could be experienced during assembly or handling. A single large diameter, thin-section four-point contact ball bearing was used to support the low speed rotor.

V. Simulated and Experimental Results

In order to characterize the torque transmission properties of the axial field magnetic gear in the AFMGM prototype, a locked HSR test was conducted by fixing the HSR in place and rotating the LSR to different angular positions. The resulting LSR torques are shown in Fig. 17 as a function of the relative electromagnetic angle (or torque angle) between the LSR and the HSR. The corresponding simulated torque characteristics obtained from static 3D FEA simulations at different torque angles are also shown in the same graph. This clearly proves that the 3D FEA model accurately predicts the gear's torque transmission capability, as the simulated and experimental results indicate a stall torque of 42.1 N·m and 42.2 N·m, respectively.

The AFMGM prototype's internal gear ratio was verified by recording the HSR speed at different LSR input speeds under the no load condition. The measurements are summarized in Fig. 18 and demonstrate a consistent gear ratio of 9.33 which matches the theoretically anticipated results based on the 28:3 pole pair combination on the rotors.

The no load, open circuit back EMF produced by the AFMGM's integrated machine was measured at several different speeds and the results are summarized by the graph in Fig. 19. The same graph also depicts the simulated back EMF amplitude characteristics obtained from a 3D FEA model. The data illustrates a high degree of consistency between the simulated and experimental results, and the relatively small deviations are likely due to a very minor difference between the actual generator air gap size and the designed size. Additional 3D FEA simulations suggest that the differences in predicted and measured back EMF amplitudes could be accounted for by less than 0.2 mm of variation in the generator air gap, which is less than 10% of the 2 mm design value.

The experimental and simulated no load, open circuit back EMF waveforms produced at an HSR speed of 1800 rpm are shown in Fig. 20. Not only are the simulated and experimental waveforms a good match for each other, but they are also very smooth sine waves with negligible harmonic content. This observation is important for two reasons, first and most importantly, it demonstrates that the AFMGM's magnetic gear and integrated generator are magnetically isolated as desired. If the two were not isolated, the EMF would contain harmonic content from the three pole pairs of the magnetic gear HSR. Second, the quality of the sine wave indicates how smoothly the HSR was rotating. This smooth operation is due in part to the lack of direct mechanical contact between the HSR and the LSR, as well as the AFMGM's low cogging torque. The HSR peak to peak torque ripple is a mere 3.5% of the HSR stall torque, while the LSR peak to peak torque ripple is only 1.3% of the LSR stall torque. These minor torque ripples are easily damped out by the machine's inertia.

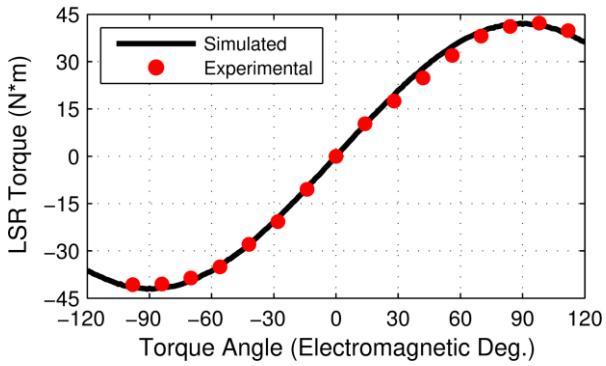

Fig. 17. AFMGM Prototype LSR Static Torque Characteristics Curve

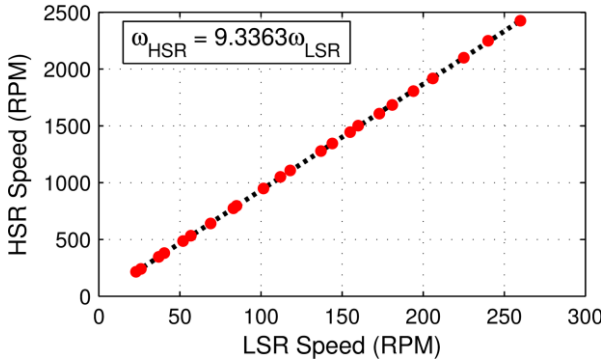

Fig. 18. AFMFGM Prototype Gear Ratio Measurements

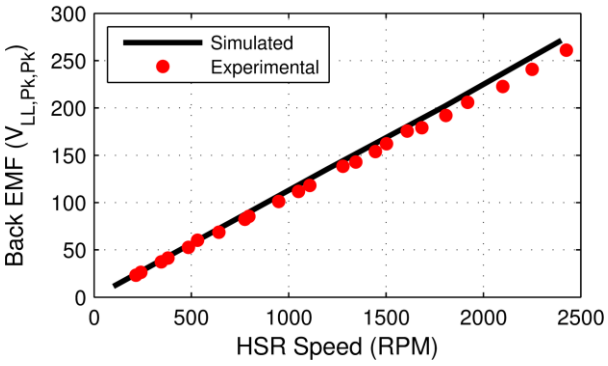

Fig. 19. Experimental and Simulated AFMGM No Load Back EMF Amplitude Characteristics

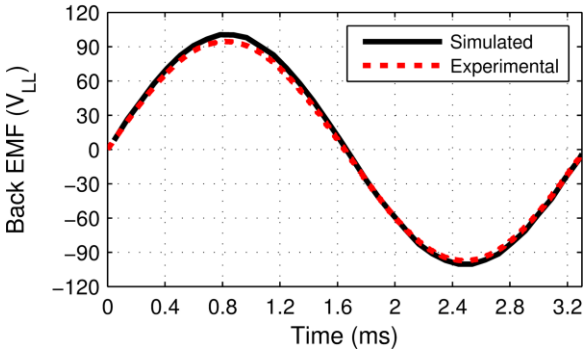

Fig. 20. Simulated and Experimental No Load Back EMF Waveforms at an HSR Speed of 1800 rpm

The AFMGM prototype's no load losses were recorded at several different LSR input speeds, and the information is shown in Fig. 21 along with the magnetic loss predictions obtained from transient 3D FEA simulations in Infolytica MagNet. This graph demonstrates that the experimental losses are significantly higher than the simulated losses. The additional losses experienced in the experimental prototype are believed to be a result of the large diameter, thin-section four-point contact bearing used on the LSR. This hypothesis is based on rotation of the individual rotors before the prototype was fully assembled. Although the strong magnetic axial forces do place a significant thrust load on both the HSR and LSR bearings, these losses are not believed to be an intrinsic characteristic of the topology, but instead an issue with this specific LSR bearing solution. In light of these findings, a modified LSR bearing arrangement was developed, and it is anticipated that this redesign would alleviate this issue.

A breakdown of the simulated no load and full load electromagnetic loss components is provided in Fig. 22. This data demonstrates that the full load and no load magnetic losses are very similar except for the iron core losses. In particular, that variation is due to the losses in the integrated generator rotor back iron, which was the only non-laminated back iron in the AFMGM. These findings suggest that with the appropriate design, the no load and full load magnetic losses should be very similar with the only significant remaining differences being the copper and mechanical losses.

The loss components breakdown in Fig. 22 also indicates that one of the largest magnetic loss components is eddy current losses produced by leakage flux in some of the structural aluminum. This was a known potential issue during the prototype development process and is primarily associated with aluminum structural reinforcement components that were added due to concerns over the large axial forces in accordance with a very conservative design approach. Based on insight gained during the prototype's construction and experimental operation, along with information from 3D mechanical FEA models, this aluminum is unnecessary and can be eliminated from future designs.

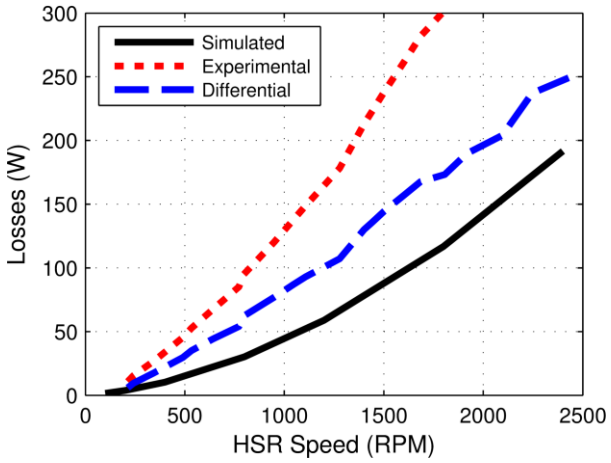

Fig. 21. Experimental and Simulated No Load AFMGM Losses

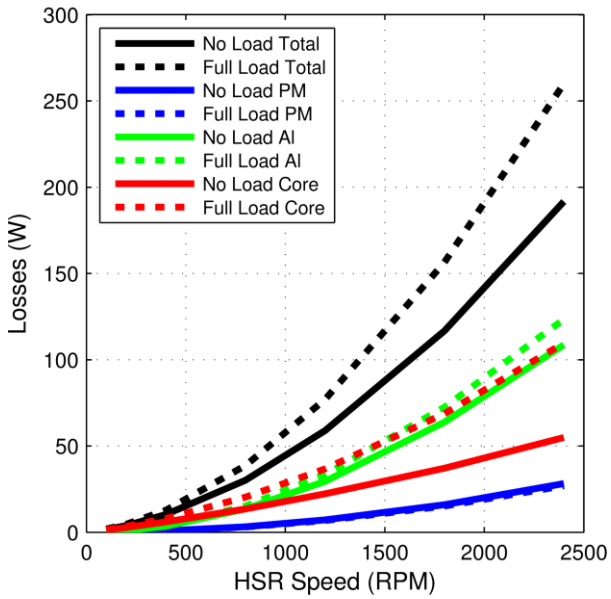

Fig. 22. Simulated No Load and Full Load Magnetic Loss Components

VI. Conclusion

A new compact axial flux magnetically geared machine topology was proposed, analyzed, prototyped, and evaluated. This AFMGM topology integrates an axial field permanent magnet machine into the bore of an axial field magnetic gear instead of connecting the two in series as was done in a previously proposed topology. Inserting the axial field machine into the bore of the axial field magnetic gear allows the two sub-systems to be optimally sized for operation with each other. This provides the potential to develop a significantly more compact AFMGM in which both the integrated machine and the magnetic gear are fully utilized to the proper extent of their individual maximum ratings. Furthermore, this integration method allows the AFMGM to have the same volume as its axial field magnetic gear, as opposed to the series combination method in which the addition of the axial field machine to the magnetic gear increases the volume of the AFMGM.

A small scale proof of concept prototype of the proposed compact AFMGM topology was developed for experimental evaluation of the device's magnetic and mechanical design and operation. The prototype AFMGM's performance was handicapped by the use of a sub-optimal commercially available axial field machine as the integrated generator and a very conservative design of the axial field magnetic gear, resulting in a low torque density of 7.8 kN·m/m^3. However, the axial field gear in the AFMGM demonstrated nearly identical torque characteristics to those predicted by 3D FEA simulations, which verifies that the modeling methods used in the design process provide an accurate means of sizing the device. Additionally, EMF data from the AFMGM's internal generator provides strong evidence that the desired magnetic isolation between the gear and the generator was achieved, as predicted by FEA simulations.

A less conservative design of the topology was simulated using the same sub-optimal integrated generator resulting in a much improved torque density of 60.6 kN·m/m^3. Although that theoretical performance is already competitive with some RFMGM designs reported in the literature, it could be further improved by redesigning both the integrated machine and axial field magnetic gear using a system level optimization. Moreover, based on the theoretical principle that the torque of an axial field magnetic gear scales with the cube of its outer radius, while its active volume only scales with the square of its outer radius, it is anticipated that higher torque densities are attainable at larger scale design points. This principle is reinforced by the 3D FEA simulation data provided in Fig. 9.

Experimental no load testing of the AFMGM prototype revealed that the device exhibited larger than anticipated no load losses. These additional losses are believed to be caused by the thin-section four-point contact bearing used on the LSR; however, this lossy bearing can be avoided in future variations of the design.

Although the prototype presented in this study exhibited a low torque density, it demonstrated the viability of the topology. Simulation results suggest that more ambitious yet still feasible designs can achieve extremely promising results. Further prototypes and experimental work are necessary to continue to refine the mechanical design and bearing arrangement and to fully characterize the scaling characteristics of the device's support structure.

ACKNOWLEDGMENT

The authors would like to thank ANSYS and Infolytica for their generous support of the EMPE lab through the provision of FEA software.

This material is based upon work supported by the Department of Energy under Award Number DE-EE0006400. This report was prepared as an account of work sponsored by an agency of the United States Government. Neither the United States Government nor any agency thereof, nor any of their employees, makes any warranty, express or implied, or assumes any legal liability or responsibility for the accuracy, completeness, or usefulness of any information, apparatus, product, or process disclosed, or represents that its use would not infringe privately owned rights. Reference herein to any specific commercial product, process, or service by trade name, trademark, manufacturer, or otherwise does not necessarily constitute or imply its endorsement, recommendation, or favoring by the United States Government or any agency thereof. The views and opinions of authors expressed herein do not necessarily state or reflect those of the United States Government or any agency thereof.

REFERENCES

[1] K. Atallah and D. Howe, "A novel high-performance magnetic gear," *IEEE Trans. Magn.*, vol. 37, no. 4, pp. 2844–2846, Jul. 2001.

[2] K. Atallah, S. D. Calverley, and D. Howe, "Design, analysis and realization of a high-performance magnetic gear," *IEE Proc. Elec. Power Appl.*, vol. 151, no.2, pp. 135–143, Mar. 2004.

[3] P. O. Rasmussen, T. O. Anderson, F. T. Jorgensen, and O. Nielsen, "Development of a High Performance Magnetic Gear," *IEEE Trans. Ind. Appl.*, vol. 41, no. 3, pp. 764-770, May-June 2005.

[4] N. W. Frank and H. A. Toliyat, "Analysis of the concentric planetary magnetic gear with strengthened stator and interior permanent magnet inner rotor," *IEEE Trans. Ind. Appl.*, vol.47, no.4, pp.1652-1660, July-Aug 2011.

[5] N. W. Frank and H. A. Toliyat, "Gearing ratios of a magnetic gear for wind turbines," in *Proc. IEEE Int. Elect. Mach. Drives Conf.*, May 3–6, 2009, pp. 1224–1230.

[6] S. Pakdelian and H. A. Toliyat, "Trans-rotary magnetic gear for wave energy applicaion," in *Power and Energy Society General Meeting*, 2012 IEEE, pp. 1-4.

[7] A. Rotondale, M. Villani, and L. Castellini, "Analysis of high-performance magnetic gears for electric vehicle," in *Proc. IEEE Int. Elect. Veh. Conf.*, Dec. 17-19, 2014, pp. 1-6.

[8] L. MacNeil, B. Claus, and R. Bachmayer, "Design and evaluation of a magnetically-geared underwater propulsion system for autonomous underwater and surface craft," in *Proc. Int. Conf. IEEE Oceans'14*, St. John's, Canada, Sep. 2014, pp. 1-8.

[9] S. Mezani, K. Atallah, and D. Howe, "A high performance axial-field magnetic gear," *J. Appl. Phys.*, vol. 99, 08R303, 2006.

[10] T. Lubin, S. Mezani, and A. Rezzoug, "Development of a 2-D Analytical Model for the Electromagnetic Computation of Axial-Field Magnetic Gears," *IEEE Trans. Magn.*, vol. 49, no. 11, pp. 5507-5521, Nov. 2013.

[11] V. M. Acharya, J. Z. Bird, and M. Calvin, "A Flux Focusing Axial Magnetic Gear," *IEEE Trans. Magn.*, vol. 49, no. 7, pp. 4092-4095, July 2013.

[12] M. Johnson, M. C. Gardner, and H. Toliyat, "Analysis of Axial Field Magnetic Gears with Halbach Arrays," in *Proc. IEEE Int. Elect. Mach. Drives Conf.*, 2015, pp 108-114.

[13] M. Johnson, A. Shapoury, P. Boghrat, M. Post, and H. A. Toliyat, "Analysis and development of an axial flux magnetic gear," in *Proc. IEEE Energy Convers. Congr. Expo*, 2014, pp. 5893-5900.

[14] K. Atallah, J. Rens, S. Mezani, and D. Howe, "A novel 'pseudo' direct-drive brushless permanent magnet machine," *IEEE Trans. Magn.*, vol. 44, no. 11, pp. 4349-4352, Nov. 2008.

[15] L. Jian, K. T. Chau, and J. Z. Jiang, "A magnetic-geared outer-rotor permanent-magnet brushless machine for wind power generation," *IEEE Trans. Ind. Appl*., vol. 35, no. 3, pp. 954–92, May–Jun. 2009.

[16] S. Gerber and R.-J. Wang, "Design of a Magnetically Geared PM Machine," in *Proc. 4th Int. Conf. Power Eng. Energy Elect. Drives*, Istanbul, Turkey, May 2013, pp. 852-857.

[17] P. O. Rasmussen, H. H. Mortensen, T. N. Matzen, T. M. Jahns, and H. A. Toliyat, "Motor integrated permanent magnet gear with a wide torque-speed range," in *Proc. IEEE Energy Convers. Congr. Expo*, 2009, pp. 1510-1518.

[18] N. Niguchi, K. Hirata, A. Zaini, and S. Nagai, "Proposal of an axial-type magnetic-geared motor," in *Proc. 20th Int. Conf. Elect. Mach*., Sep. 2012, pp. 738-743

[19] C. Tong, Z. Song, P. Zheng, J. Bai, and Q. Zhao, "Research on Electromagnetic Performance of an Axial Magnetic-Field-Modulated Brushless Double-Rotor Machine for Hybrid Electric Vehicles," *in Proc. 17th Int. Conf. Elect. Mach. Syst.*, Hangzhou, China, Oct 2014, pp. 2896-2902.

[20] W. N. Fu and S. L. Ho, "A novel axial-flux electric machine for in-wheel gearless drive in plug-in hybrid electric vehicles," in *Proc. IEEE Conf. Electromagnetic Field Computation*, Chicago, IL, May 2010.

[21] R.-J. Wang, L. Brönn, S. Gerber, and P. M. Tlali, "Design and evaluation of a disc-type magnetically geared PM wind generator," in *Int. Conf. Power Eng., Energy & Electr. Drives*, pp.1259-1264, 2013.

[22] L. Brönn, "Design and Performance Evaluation of a Magnetically Geared Axial-Flux Permanent Magnet Generator," M.S. Thesis, Dept. Elect. Eng., Stellenbosch Univ., Stellenbosch, South Africa, 2012.

[23] M. Johnson, M. C. Gardner and H. A. Toliyat, "Design and analysis of an axial flux magnetically geared generator," in *Proc. IEEE Energy Convers. Congr. Expo*, 2015, pp. 6511-6518.